*photonics*

MDPI

*Article*

# Precision Spectroscopy of Radiation Transitions between Singlet Rydberg States of the Group IIb and Yb Atoms

**Igor L. Glukhov [1,*], Aleksandr A. Kamenski [1], Vitaly D. Ovsiannikov [1,2] and Vitaly G. Palchikov [2,3]**

[1] Faculty of Physics, Voronezh State University, Voronezh 394018, Russia; san40@bk.ru (A.A.K.); ovd@phys.vsu.ru (V.D.O.)
[2] Federal State Unitary Enterprise "VNIIFTRI", Mendeleevo 141570, Russia; vitpal@mail.ru
[3] Laser Plasma Institute, National Research Nuclear University MEPhI, Moscow 115409, Russia
* Correspondence: glukhov@phys.vsu.ru

**Abstract:** The measurements of microwave (μw) and radio-frequency (RF) radiation quantitative parameters may be based on the quantum–optical approach to determine the spectral characteristics of radiation transitions between the Rydberg states of atoms. Frequencies and matrix elements are calculated for dipole transitions between opposite-parity Rydberg states $n^1L_L$ and $n'^1(L \pm 1)_{L\pm1}$ (where $n' = n, n \pm 1, n \pm 2$) of the singlet series in the alkaline–earth–metal-like atoms of group IIb (Zn, Cd, Hg) and Yb. The matrix elements determine the shifts of Rydberg-state energy levels in the field of resonance μw or RF radiation, splitting the resonance of electromagnetically induced transparency (EIT) for intensely absorbed probe radiation. Numerical computations based on the single-electron quantum defect method (QDM) and the Fues' model potential (FMP) approach with the use of the most reliable data from the current literature on quantum defect values are performed for frequencies and matrix elements of transitions between singlet Rydberg states of $^1S_0$-, $^1P_1$-, $^1D_2$-, and $^1F_3$-series in Zn, Cd, Hg, and Yb atoms. The calculated data are approximated by polynomials in the powers of the principal quantum numbers. The polynomial coefficients are determined with the use of a standard curve-fitting interpolation polynomial procedure for numerically calculated functions. These approximation expressions provide new possibilities for accurately evaluating the frequencies and matrix elements of dipole transitions between Rydberg states over a wide range of quantum numbers $n >> 1$, accompanied by the emission and absorption of μw and RF photons.

**Keywords:** microwave (μw) radiation; dipole transitions; Rydberg states; alkaline–earth–metal atoms



**Citation:** Glukhov, I.L.; Kamenski, A.A.; Ovsiannikov, V.D.; Palchikov, V.G. Precision Spectroscopy of Radiation Transitions between Singlet Rydberg States of the Group IIb and Yb Atoms. *Photonics* **2023**, *10*, 1153. https://doi.org/10.3390/photonics10101153

Received: 15 August 2023
Revised: 4 October 2023
Accepted: 11 October 2023
Published: 13 October 2023



## 1. Introduction

The use of atomic quantum properties and characteristics is currently the most reliable approach to developing the highest precision set of metrological standards. Time-frequency standards, based on neutral atoms, represent the most spectacular examples of metrological standards with record fractional uncertainties below $10^{-18}$, continuously attracting significant attention from researchers [1–3].

The splitting of the electromagnetically induced transparency (EIT) resonance in atoms in the field of infrared (IR), microwave (μw), or radio-frequency (RF) radiation may be used as a method for high-precision determination of the quantitative characteristics of electric fields in the indicated spectral ranges [4–9]. The frequencies of the radiation transitions between the single-electron Rydberg states of atoms are located exactly in these ranges. Therefore, the alkali-metal atoms with their single valence electrons, which may be easily excited to their Rydberg states without disturbing electrons from the inner shells, were the first to attract the attention of researchers involved in the development of atomic standards for the μw electric fields. The basic atomic characteristics in these studies were the amplitudes and frequencies of the radiation transitions between the Rydberg states. Detailed calculations of these characteristics for alkali-metal atoms (Li, Na, K, Rb, and Cs)

were performed in [10]. Similar results for the alkaline–earth–metal atoms of group IIa (Mg, Ca, Sr, and Ba) were obtained in [11]. In this paper, we present similar calculations for the group IIb (Zn, Cd, and Hg) and Yb atoms. Our aim is to derive simple equations for determining the numerical data for the frequencies and amplitudes of radiation transitions between singlet Rydberg states.

Currently, existing databases on the energies of atomic bound states may serve as a source for determining the frequencies of radiation transitions between the Rydberg states of atoms. Modern laser systems provide access and the detection of highly excited states with the use of methods of multiphoton transition spectroscopy [4,12]. The states $n^1\mathrm{F}_3$, $n^1\mathrm{D}_2$, $n^1\mathrm{P}_1$, and $n^1\mathrm{S}_0$ are the most suitable for observing μw transitions in alkaline–earth–metal-like atoms because, in close vicinity of their energies, there exist states $n'^1\mathrm{L}'_{\mathrm{L}'}$ dipole transitions, which are located in Tera-, Giga-, and Mega-Hertz frequency ranges.

In the most reliable databases, the numerical values of energy levels for the *n*S-, *n*P-, *n*D- and *n*F-series are given only for a finite number of states with $n \leq n_{\max}$, where $n_{\max}$ depends essentially on the orbital momentum of the series presented in a particular database for a specific atom [13,14]. In particular, for Zn and Hg atoms, the total number of tabulated energy levels in the database [14] is approximately 1.5 times the number $n_{\max}$ of the base [13]. For Cd and Yb atoms, the total number of tabulated items in the database [14] is approximately three times the corresponding number of the base [13]. Therefore, the numbers $n_{\max}$ for a particular series of states may also differ in bases similar to the indicated proportions. However, due to the limited digit numbers used for the numerical presentation of energy levels in the data tables, the uncertainty of the numerical values for the parameters determining transition frequencies and matrix elements gradually decreases with increasing corresponding Rydberg-state principal quantum numbers $n$. Therefore, the values $n < 40$ are usually sufficient for determining the wave function and transition–energy parameters with a precision of four to five digits.

The frequencies of the most intensely absorbed lines of the alkaline–earth–metal-like atoms are determined by the energy of transitions from their ground states $n_0{}^1\mathrm{S}_0$ to the first excited singlet states $n_0{}^1\mathrm{P}_1$, where $n_0 = 4$, 5, 6, and 6 are the principal quantum numbers of group IIb (Zn, Cd, Hg) and Yb atoms, respectively. The EIT effect on the probe radiation with the frequency $\omega_{\mathrm{p}} = E_{n_0{}^1\mathrm{P}_1} - E_{n_0{}^1\mathrm{S}_0}$ in the atomic vapor appears under the action of sufficiently strong laser radiation, coupling the excited state $n_0{}^1\mathrm{P}_1$ to a highly excited Rydberg state $n^1\mathrm{L}_{\mathrm{L}}$ with a principal quantum number $n \gg n_0$. The subscript at the angular momentum L determines the quantum number J of the total orbital momentum $\mathbf{J} = \mathbf{L} + \mathbf{S}$, which for spin-less singlet states $\mathbf{S} = 0$, coincides exactly with the angular momentum J = L. In the case of a single-photon coupling, the Rydberg-state angular momentum equals 0 or 2. If the Rydberg-state excitation requires $\mathrm{N} \geq 1$ photon, for an even number of N = 2, 4, . . ., the Rydberg-state angular momentum may take only odd values from L = 1 to L = N + 1. For odd photon numbers N = 1, 3, . . ., the angular momentum takes even values from L = 0 to L = N + 1 = 2, 4, . . . [12]. The photons may be identical, coming from one and the same coupling laser beam of the frequency $\omega_i \equiv \omega_{\mathrm{c}}$, $i = 1, 2, \ldots N$, or different, coming from N different coupling beams of the frequencies $\omega_i \neq \omega_k$, $i \neq k = 1, 2, \ldots N$. The resonance of the EIT effect appears when the sum of all coupling laser frequencies $\omega_\Sigma = \sum_{i=1}^{N} \omega_i$ coincides exactly with the frequency of transition from the opaque excited state $n_0{}^1\mathrm{P}_1$ to the Rydberg state $n^1\mathrm{L}_{\mathrm{L}}$, i.e., $\omega_\Sigma \equiv E_{n^1\mathrm{L}_{\mathrm{L}}} - E_{n_0{}^1\mathrm{P}_1} = E_{n^1\mathrm{L}_{\mathrm{L}}} - E_{n_0{}^1\mathrm{S}_0} - \omega_{\mathrm{p}}$. It is important to note that, in the case of multiple coupling beams, there may be both absorbed and emitted photons, and then the corresponding frequencies $\omega_i$ in the sum $\omega_\Sigma$ are positive for the former and negative for the latter. The splitting of the EIT resonance using μw radiation may be used for determining the basic characteristics of Rydberg states in atoms, frequencies, and amplitudes of dipole transitions between close Rydberg states.

If, together with the coupling laser field, a μw radiation (IR or RF radiation, for which in what follows we use one and the same notation μw) is applied with a frequency $\omega_{\mu\mathrm{w}} \equiv E_n - E_{n'} - \varepsilon$ close to the frequency of the $n \to n'$ transition ($|\varepsilon| \ll \omega_{\mu\mathrm{w}}$) between Rydberg states $\left|n^1\mathrm{L}_{\mathrm{L}}\right\rangle$ and $\left|n'^1\mathrm{L}'_{\mathrm{L}'}\right\rangle$ with $\mathrm{L}' = \mathrm{L} \pm 1$, $n' = n, n \pm 1, n \pm 2$, then the state

$n^1\mathrm{L}_\mathrm{L}$ transforms into two possible superpositions of states due to the resonance Stark effect (the Autler–Towns effect [15]). The essential details and general equations for this effect are presented in Section 2.

The frequencies and corresponding matrix elements are determined for the μw dipole transitions between the singlet Rydberg states of the alkaline–earth–metal-like atoms of group IIb elements (Zn, Cd, and Hg) and Yb. The most reliable data on the energy spectra and quantum defects of the $n^1\mathrm{S}_0$-, $n^1\mathrm{P}_1$-, $n^1\mathrm{D}_2$-, and $n^1\mathrm{F}_3$-series of bound states are used to evaluate the frequencies of the μw transitions between the Rydberg states. The numerical results of the calculations and their extrapolations to states with extremely large principal quantum numbers $n$ are presented in Section 3. The values of the μw transition matrix elements $\mathcal{R}$ are calculated in the single-electron approximation using the Fues' model potential (FMP) and the quantum defect method (QDM). The numerical results and quadratic polynomial approximations for evaluating the amplitudes of transitions between Rydberg states are presented in Section 4. In Section 5, the results of numerical calculations are discussed.

## 2. μw-Radiation-Induced Splitting of EIT Resonance

The energies of the Rydberg-state superpositions in the field of resonant μw radiation are determined as solutions to the secular equation for degenerate quasienergy states the following [16–18]:

$$E_n^{\pm} = E_{n^1\mathrm{L}_\mathrm{L}} \pm \Delta E(\varepsilon, \Omega), \tag{1}$$

with the Autler–Towns resonance splitting

$$\Delta E(\varepsilon, \Omega) = \frac{1}{2}\sqrt{\varepsilon^2 + \Omega^2}, \tag{2}$$

where $\Omega = F\mathcal{R}$ is the amplitude of the μw transition between Rydberg states $|n\rangle$ and $|n'\rangle$ (the "Rabi frequency"), $F$ is the μw electric field, $\mathcal{R} = \langle n'|z|n\rangle$ is the matrix element of the electric dipole moment $z$-component (hereafter, the atomic system of units used is $e = m = \hbar = 1$).

For the EIT resonance condition,

$$\omega_\mathrm{p} + \omega_\Sigma = E_{n^1\mathrm{L}_\mathrm{L}} - E_{n_0{}^1\mathrm{S}_0}, \tag{3}$$

the μw-induced splitting of the Rydberg-state energy (1), and (2) will evidently result in the EIT resonance splitting for the probe radiation $\omega_\mathrm{p} \to \omega_\mathrm{p}^{\pm} + \Delta\omega^{\pm}$. Then, the relation (3) transforms into resonance conditions for two separate resonances as follows:

$$\omega_\mathrm{p}^{+} + \omega_\Sigma = E_n^{+} - E_{n_0{}^1\mathrm{S}_0}, \text{ and } \omega_\mathrm{p}^{-} + \omega_\Sigma = E_n^{-} - E_{n_0{}^1\mathrm{S}_0}, \tag{4}$$

where $E_n^{\pm}$ are determined in (1) and (2). The difference between these relations determines the splitting of the EIT resonances $\Delta\omega_\mathrm{p} = \omega_\mathrm{p}^{+} - \omega_\mathrm{p}^{-} = 2\Delta E(\varepsilon, \Omega)$ observed at the probe-wave frequencies $\omega_\mathrm{p}^{\pm} = \omega_\mathrm{p} \pm \Delta E(\varepsilon, \Omega)$. It is necessary to note that in the case of collinear propagation of the probe and coupling beams, the linear Doppler effect on the frequencies $\omega_\mathrm{p}$ and $\omega_\Sigma$ is one and the same for both frequencies $\omega_\mathrm{p}^{+}$ and $\omega_\mathrm{p}^{-}$; therefore, it cancels out their difference $\Delta\omega_\mathrm{p}$ [10,11]. Thus, the probe-wave resonance splitting coincides exactly with twice the resonance shift (2), enabling the determination of the μw radiation electric field $F$ from the EIT resonance splitting. The total number of Rydberg states in atoms is practically infinite, whereas the selection of probe $\omega_\mathrm{p}$ and coupling $\omega_\Sigma$ laser frequencies providing the multi-photon transition from the ground state to the Rydberg $n^1\mathrm{L}_\mathrm{L}$ state is not too difficult [4,12]. Therefore, the measurements of any μw radiation field $F$ may always be realized by choosing four bound states (ground $n_0{}^1\mathrm{S}_0$, resonance $n_0{}^1\mathrm{P}_1$, and a pair of Rydberg states $n$ and $n'$) together with a number of resonant coupling beams. For an exact coincidence of the frequency $\omega_{\mu\mathrm{w}}$ with the frequency of the transition between Rydberg states (that is, for $\varepsilon = 0$ in $\Delta E(\varepsilon, \Omega)$ of Equation (2)), the splitting $\Delta\omega_\mathrm{p}$ coincides

with the Rabi frequency Ω. Then, the electric field of μw radiation with a frequency exactly equal to the transition frequency $\omega_{\mu w} = |E_n - E_{n'}|$ is as follows:

$$F = \Omega/\mathcal{R}, \tag{5}$$

This relation holds for all atoms in an atomic vapour, independent of the vapour temperature, if all laser beams (probe and coupling) co- or counter-propagate along one and the same line with coinciding directions of their linearly polarized electric field vectors [6–11,17] (see Figure 1a). So, for the counter-propagating probe and coupling waves, the Doppler-effect-insensitive difference $\Delta\omega_p$ remains equal to $2\Delta E(\varepsilon, \Omega)$ for all atoms in the laboratory reference frame, independent of the atomic thermal velocities.

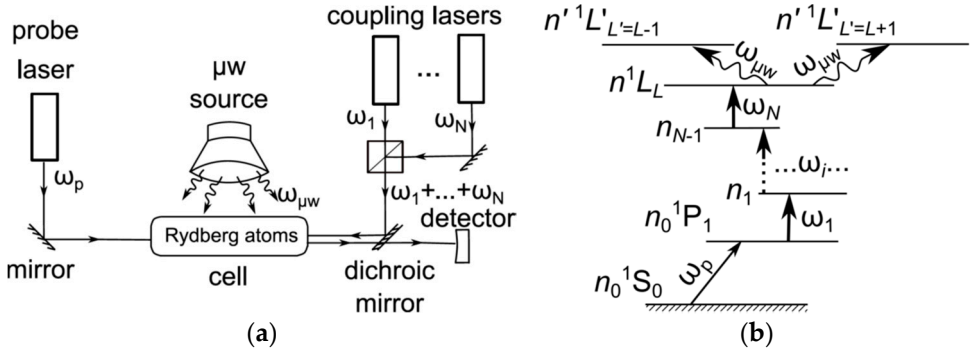


**Figure 1.** (**a**) Schematic of the probe laser radiation ($\omega_p$), coupling beams (of the summary frequency $\omega_\Sigma = \sum_{i=1}^{N} \omega_i$), and μw ($\omega_{\mu w}$) radiation; (**b**) the energy-level scheme for the N-photon excitation of the Rydberg $n$L state and the splitting of the EIT resonance using a beam of μw radiation resonant to the $n\mathrm{L} \to n'\mathrm{L}'$ ($\mathrm{L}' = \mathrm{L} \pm 1$) transitions.

Thus, for a given frequency of μw radiation in the frequency ranges of MHz, GHz up to a few THz, Rydberg state $n^1\mathrm{L}_\mathrm{L}$ should be determined with a close $n'^1\mathrm{L}'_{\mathrm{L}'}$ state ($\mathrm{L}' = \mathrm{L} \pm 1$), providing equality $\omega_{\mu w} = |E_n - E_{n'}|$. After calculation of the matrix element $\mathcal{R} = \langle n'|z|n\rangle$ the μw electric field may be evaluated using Equation (5), where the experimentally determined values of the EIT resonance splitting $\Delta\omega_p$ should substitute the Rabi frequency Ω.

## 3. Frequencies of μw Transitions between Rydberg States of Alkaline–Earth–Metal-like Atoms

The difference between the energy of $n'^1\mathrm{L}'_{\mathrm{L}'}$ and $n^1\mathrm{L}_\mathrm{L}$ levels for $\mathrm{L}' = \mathrm{L} \pm 1$ and $|n' - n| \leq 2$ vanishes as $1/n^3$ with an increase in the principal quantum number $n$. Therefore, the determination of transition energy from tables of energy levels becomes impossible already for $n > 20$, since the terms in the relations $\Delta E_{n\mathrm{LL}'} = E_{n'^1\mathrm{L}'_{\mathrm{L}'}} - E_{n^1\mathrm{L}_\mathrm{L}}$ differ only in the 6th or 7th digit number for $n > 15$. Thus, for the most precise determination of $\Delta E_{n\mathrm{LL}'}$ the data for quantum defects of the bound states should be used. The definition of the quantum defect $\mu_{n\mathrm{L}}$ with a principal quantum number $n$ and orbital quantum number L is based on the Rydberg equation for the bound-state energy (in the units of $\mathrm{cm}^{-1}$):

$$E_{n\mathrm{L}} = Ip_A - \frac{Ry_A}{(n - \mu_{n\mathrm{L}})^2}, \tag{6}$$

with $Ip_A$, the energy of a single-electron ionization of an atom from its ground state, $Ry_A = Ry_\infty/(1 + 1/M_A)$, is the Rydberg constant, taking into account the finite mass $M_A$ of atom $A$ in the units of the electron mass, $Ry_\infty = 109,737.315685\ \mathrm{cm}^{-1}$ is the universal Rydberg constant (for $M_A = \infty$) given by the CODATA recommended values of the fundamental constants (https://physics.nist.gov/Constants (accessed on 25 August 2023)).

The quantum defect $\mu_{n\mathrm{L}}$ for a series of states with a fixed orbital momentum L is practically independent of the principal quantum number $n$ ($\mu_{n\mathrm{L}} \approx \mu_0$ [19]) in the region of $n > 20$ and may be presented as a resolution of the form [20,21].

$$\mu_{n\mathrm{L}} = \sum_{q=0}^{q_{\max}} \frac{\mu_{2q}}{(n-\mu_0)^{2q}}, \tag{7}$$

where $\mu_{2q}$ ($q = 0, 1, 2, \ldots, q_{\max}$) are constant parameters for a series of states with fixed values of the total spin S and angular momentum L. In this paper, we considered only singlet states with total spin S = 0. A sufficient number of theoretical and experimental studies were performed to determine the numerical values of constants $\mu_{2q}$, $Ip_A$, and $Ry_A$ [20–24], providing high-precision values of the bound-state energies (6) in alkaline–earth–metal-like atoms of group IIb ($A$ = Zn, Cd, and Hg) and Yb.

In Table 1, the most reliable values of constants $\mu_{2q}$ are presented, taken from the literature and those derived from Equation (6) using the data [13,14] for Rydberg-state energies. From the numerical values of $\mu_{2q}$, for $n > 15$, the main contribution to the sum (7) comes from the two terms $q = 0.1$. We verified the data of Table 1 via a detailed comparison of the energies given by Equation (6) with those of the databases [13,14]. The coincidence of the compared values up to the last digits for all considered atoms confirms the high precision of the calculated results for frequencies and matrix elements presented below.

**Table 1.** Numerical data for constants of Equations (6) and (7) determining quantum defects and energies of alkaline–earth–metal-like atom singlet Rydberg states.

| **Series** $n\,^1\mathrm{L_J}$ | $\mu_{2q}$ | **Atom (and Its Ground State)** | | | |
|---|---|---|---|---|---|
| | | **Zn ($3d^{10}\,4s^2$ ($^1S_0$))** | **Cd ($4d^{10}\,5s^2$ ($^1S_0$))** | **Hg ($5d^{10}6s^2$($^1S_0$))** | **Yb ($4f^{14}\,6s^2$ ($^1S_0$))** |
| $n\,^1\mathrm{S}_0$ | $\mu_0$ | 2.642512 | 3.663305 | 4.67192 | 4.28365 |
| | $\mu_2$ | −2.89467 | −6.11623 | −6.02082 | −10.3200 |
| | $\mu_4$ | 104.771 | 108.891 | 144.630 | −70.1351 |
| $n\,^1\mathrm{P}_1$ | $\mu_0$ | 2.09749 | 3.0583 | 4.06980 | 3.97663 |
| | $\mu_2$ | −1.6302 | −2.0660 | −8.33250 | −6.0866 |
| | $\mu_4$ | 86.502 | 155.708 | 185.691 | 162.57 |
| $n\,^1\mathrm{D}_2$ | $\mu_0$ | 1.231886 | 2.22767 | 3.10517 | 2.721 |
| | $\mu_2$ | −2.51951 | −0.932065 | −3.3896 | −2.0871 |
| | $\mu_4$ | 131.023 | −39.03163 | 97.3023 | −19.7052 |
| $n\,^1\mathrm{F}_3$ | $\mu_0$ | 0.02302346 | 0.0368361 | 1.05146 | 1.2894 |
| | $\mu_2$ | 0.188324 | 0.027443 | −3.4951 | −7.869 |
| | $\mu_4$ | −4.61722 | −3.54482 | 119.614 | 84.757 |
| $Ry_\mathrm{A}$ ($\mathrm{cm}^{-1}$) | | 109,736.395 | 109,736.7802 | 109,737.0156 | 109,736.9677 |
| $Ip_\mathrm{A}$ ($\mathrm{cm}^{-1}$) | | 75,769.33 | 72,540.07 | 84,184.15 | 50,443.0704 |

The numerical values of frequencies are presented In Tables 2–5 for the μw dipole radiation transitions from the EIT-resonance-stimulating Rydberg $n^1$L states with L = 0, 1, 2, 3 and some specific values of the principal quantum number in the region of $20 \leq n \leq 200$ to $n'^1$L′ states of group IIb and Yb atoms. The notations used for the letters in subscripts of the quantities $\Delta E_{n\mathrm{LL}'}$ are as follows: the first letter $n$ determines the principal quantum number of the $n^1$L Rydberg state; the second letter L determines the angular momentum of the higher-energy state in the μw radiation transition; the third letter L′ determines the angular momentum of the state with lower energy.

**Table 2.** Frequencies of electric dipole transitions between Rydberg states of ***Zn*** atoms: from $n^1S_0$ to $(n-1)^1P_1$ state, $\Delta E_{n\mathrm{SP}} = E_{n^1S_0} - E_{(n-1)^1P_1}$; from $n^1P_1$ to $n^1S_0$ state, $\Delta E_{n\mathrm{PS}} = E_{n^1P_1} - E_{n^1S_0}$; from $(n+1)^1P_1$ to $n^1D_2$ state, $\Delta E_{n\mathrm{PD}} = E_{(n+1)^1P_1} - E_{n^1D_2}$; from $n^1D_2$ to $(n-2)^1F_3$ state, $\Delta E_{n\mathrm{DF}} = E_{n^1D_2} - E_{(n-2)^1F_3}$; from $(n-1)^1F_3$ to $n^1D_2$ state, $\Delta E_{n\mathrm{FD}} = E_{(n-1)^1F_3} - E_{n^1D_2}$.

| $n$ | $\Delta E_{n\mathrm{SP}}$, GHz | $\Delta E_{n\mathrm{PS}}$, GHz | $\Delta E_{n\mathrm{PD}}$, GHz | $\Delta E_{n\mathrm{DF}}$, GHz | $\Delta E_{n\mathrm{FD}}$, GHz |
|---|---|---|---|---|---|
| 20 | 600.0652 | 648.970 | 130.054 | 846.8076 | 197.921 |
| 50 | 28.6296 | 33.1524 | 7.57120 | 46.0590 | 11.7095 |
| 100 | 3.26784 | 3.85265 | 0.915272 | 5.47010 | 1.41991 |
| 150 | 0.940038 | 1.11441 | 0.268122 | 1.59392 | 0.416259 |
| 200 | 0. 390809 | 0.464549 | 0.112467 | 0.666882 | 0.174659 |
| Parameters of interpolation Equation (8) | | | | | |
| $d_0$, THz | 3001.46 | 3588.88 | 884.234 | 5207.72 | 1374.16 |
| $d_1$ | 8.07501 | 6.94763 | 3.50412 | 4.79019 | 3.40025 |
| $d_2$ | 78.2588 | 39.6976 | 0.576217 | 24.5359 | −7.10743 |

**Table 3.** Frequencies of electric dipole transitions between Rydberg states of ***Cd*** atoms: from $n^1S_0$ to $(n-1)^1P_1$ state, $\Delta E_{n\mathrm{SP}} = E_{n^1S_0} - E_{(n-1)^1P_1}$; from $n^1P_1$ to $n^1S_0$ state, $\Delta E_{n\mathrm{PS}} = E_{n^1P_1} - E_{n^1S_0}$; from $(n+1)^1P_1$ to $n^1D_2$ state, $\Delta E_{n\mathrm{PD}} = E_{(n+1)^1P_1} - E_{n^1D_2}$; from $n^1D_2$ to $n^1P_1$ state, $\Delta E_{n\mathrm{DP}} = E_{n^1D_2} - E_{n^1P_1}$; from $(n-2)^1F_3$ to $n^1D_2$ state, $\Delta E_{n\mathrm{FD}} = E_{(n-2)^1F_3} - E_{n^1D_2}$.

| $n$ | $\Delta E_{n\mathrm{SP}}$, GHz | $\Delta E_{n\mathrm{PS}}$, GHz | $\Delta E_{n\mathrm{PD}}$, GHz | $\Delta E_{n\mathrm{DP}}$, GHz | $\Delta E_{n\mathrm{FD}}$, GHz |
|---|---|---|---|---|---|
| 20 | 641.336 | 839.645 | 197.410 | 1043.09 | 216.158 |
| 50 | 26. 5831 | 39.1125 | 10.1946 | 51.4334 | 11.4226 |
| 100 | 2.92795 | 4.40750 | 1.19009 | 5.92182 | 1.33881 |
| 150 | 0.833096 | 1.26206 | 0.344878 | 1.70794 | 0.388282 |
| 200 | 0.344515 | 0.523459 | 0.143906 | 0.710946 | 0.162065 |
| Parameters of interpolation Equation (8) | | | | | |
| $d_0$, THz | 2624.22 | 3987.14 | 1114.65 | 5475.17 | 1255.61 |
| $d_1$ | 9.60881 | 9.74238 | 6.37655 | 7.56129 | 6.39761 |
| $d_2$ | 189.875 | 79.0349 | 39.2051 | 58.4159 | 22.9400 |

**Table 4.** Frequencies of electric dipole transitions between Rydberg states of ***Hg*** atoms: from $n^1S_0$ to $(n-1)^1P_1$ state, $\Delta E_{n\mathrm{SP}} = E_{n^1S_0} - E_{(n-1)^1P_1}$; from $n^1P_1$ to $n^1S_0$ state, $\Delta E_{n\mathrm{PS}} = E_{n^1P_1} - E_{n^1S_0}$; from $(n+1)^1P_1$ to $n^1D_2$ state, $\Delta E_{n\mathrm{PD}} = E_{(n+1)^1P_1} - E_{n^1D_2}$; from $n^1D_2$ to $n^1P_1$ state, $\Delta E_{n\mathrm{DP}} = E_{n^1D_2} - E_{n^1P_1}$; from $(n-2)^1F_3$ to $n^1D_2$ state, $\Delta E_{n\mathrm{FD}} = E_{(n-2)^1F_3} - E_{n^1D_2}$.

| $n$ | $\Delta E_{n\mathrm{SP}}$, GHz | $\Delta E_{n\mathrm{PS}}$, GHz | $\Delta E_{n\mathrm{PD}}$, GHz | $\Delta E_{n\mathrm{DP}}$, GHz | $\Delta E_{n\mathrm{FD}}$, GHz |
|---|---|---|---|---|---|
| 20 | 721.729 | 1045.17 | 69.8134 | 1404.05 | 72.8383 |
| 50 | 28. 3622 | 41.7668 | 2.39541 | 63.3287 | 3.42273 |
| 100 | 3.03030 | 4.53200 | 0.259470 | 7.07836 | 0.388177 |
| 150 | 0.853440 | 1.28298 | 0.0738689 | 2.02177 | 0.111430 |
| 200 | 0.351132 | 0.529215 | 0.0305908 | 0.837533 | 0.0462760 |
| Parameters of interpolation Equation (8) | | | | | |
| $d_0$, THz | 2624.05 | 4002.39 | 239.444 | 6365.83 | 354.146 |
| $d_1$ | 13.3090 | 11.0088 | 3.55212 | 10.1445 | 8.76692 |
| $d_2$ | 213.961 | 215.459 | 461.965 | 102.902 | 82.8157 |

**Table 5.** Frequencies of electric dipole transitions between Rydberg states of **Yb** atoms: from $n^1S_0$ to $(n-1)^1P_1$ state, $\Delta E_{n\mathrm{SP}} = E_{n^1S_0} - E_{(n-1)^1P_1}$; from $n^1P_1$ to $n^1S_0$ state, $\Delta E_{n\mathrm{PS}} = E_{n^1P_1} - E_{n^1S_0}$; from $n^1D_2$ to $(n+1)^1P_1$ state, $\Delta E_{n\mathrm{DP}} = E_{n^1D_2} - E_{(n+1)^1P_1}$; from $n^1D_2$ to $(n-2)^1F_3$ state, $\Delta E_{n\mathrm{DF}} = E_{n^1D_2} - E_{(n-2)^1F_3}$; from $(n-1)^1F_3$ to $n^1D_2$ state, $\Delta E_{n\mathrm{FD}} = E_{(n-1)^1F_3} - E_{n^1D_2}$.

| $n$ | $\Delta E_{n\mathrm{SP}}$, GHz | $\Delta E_{n\mathrm{PS}}$, GHz | $\Delta E_{n\mathrm{DP}}$, GHz | $\Delta E_{n\mathrm{DF}}$, GHz | $\Delta E_{n\mathrm{FD}}$, GHz |
|---|---|---|---|---|---|
| 20 | 1283.50 | 466.948 | 317.260 | 733.479 | 549.900 |
| 50 | 48. 9559 | 20.7817 | 15.9336 | 35.8654 | 26.6549 |
| 100 | 5.25988 | 2.28902 | 1.83149 | 4.09419 | 3.06835 |
| 150 | 1.48466 | 0.650409 | 0.527554 | 1.17700 | 0.885485 |
| 200 | 0.611535 | 0.268725 | 0.219433 | 0.489114 | 0.368745 |
| Parameters of interpolation Equation (8) | | | | | |
| $d_0$, THz | 4627.60 | 2017.90 | 1682.17 | 3741.20 | 2847.36 |
| $d_1$ | 10.8572 | 12.5539 | 8.55139 | 8.95025 | 6.95394 |
| $d_2$ | 270.400 | 89.4135 | 32.4966 | 48.3700 | 78.9251 |

The standard procedure of the curve fitting polynomial interpolation was used for the calculated data to derive analytical equations for the transition energy as functions of the $n^1L_L$ state principal quantum number in the following form:

$$\Delta E_{n\mathrm{LL}'} = \frac{d_0}{n^3}\left(1 + \frac{d_1}{n} + \frac{d_2}{n^2}\right). \quad (8)$$

The coefficients $d_0$, $d_1$, and $d_2$, presented in Tables 2–5, were determined from specific numerical values of the transition energy $\Delta E_{n\mathrm{LL}'}$ for $n$ = 20, 60, and 120. Evidently, the coefficients of $d$ are closely related to coefficients $\mu_{2q}$ of resolution (5) for the quantum defects of states $n^1L$ and $n'^1L'$. Nevertheless, the straightforward use of the calculated data for transition frequencies appears more efficient for deriving the $d$ coefficients of the asymptotic presentation (8). This conclusion follows from the fact that the quantum defects (7) are determined from energies (6) of only one and the same series of states with a fixed orbital quantum number L, whereas the transition energies (8) involve energies of two separate series of states with different orbital momenta L and L′, and therefore with different quantum defects (7), involving implicitly terms of higher orders of the number $q > q_{\max}$.

## 4. Amplitudes of the μw Dipole Transitions between the Singlet Rydberg States of the Alkaline–Earth–Metal-like Atoms

The matrix element $\mathcal{R} = \langle n'|z|n\rangle$ of the single-electron dipole radiation transition between highly excited Rydberg states may be calculated using the standard methods of atomic spectroscopy [17,19]. Let the $z$-axis point along the polarization vectors of all linearly polarized radiation beams, i.e., the probe, coupling, and μw electromagnetic waves. Then, the $z$-axis may be considered as a quantization axis for the initial (ground) $n_0{}^1S_0$ state, resonance $n_0{}^1P_1$, and Rydberg $n^1L_L$ and $n'^1L'_{L'}$ states. Therefore, the magnetic quantum numbers of all involved states coincide with the $z$-component of the total angular momentum of the ground state $M_0 = 0$. After integration over angular variables with the use of the quantum theory of angular momentum [25], the μw transition matrix element may be presented in terms of the radial matrix element $\langle n'L'|r|nL\rangle$, as follows:

$$\mathcal{R} = \frac{\mathrm{L}+\mathrm{L}'+1}{2\sqrt{(2\mathrm{L}+1)(2\mathrm{L}'+1)}}\langle n'\mathrm{L}'|r|n\mathrm{L}\rangle. \tag{9}$$

The radial matrix element $\langle n'\mathrm{L}'|r|n\mathrm{L}\rangle$ in this equation may be calculated using one of the well-known semi-empirical methods, the Fues' Model Potential (FMP), or the Quantum Defect Method (QDM) [17,19]. In both methods, the radial wave functions may be presented in terms of polynomials in powers of their arguments

$$R^{(\mathrm{FMP})}_{n\mathrm{L}}(r) = \frac{2Z^{3/2}}{\nu^2_{n\mathrm{L}}}\sqrt{\frac{n_r!}{\Gamma(\nu_{n\mathrm{L}}+\lambda+1)}}\exp\left(-\frac{x}{2}\right)x^{\lambda}L^{2\lambda+1}_{n_r}(x); \tag{10}$$

$$R^{(\mathrm{QDM})}_{n\mathrm{L}}(r) = \frac{2Z^{3/2}}{\nu^2_{n\mathrm{L}}\sqrt{\Gamma(\nu_{n\mathrm{L}}+\mathrm{L}+1)\Gamma(\nu_{n\mathrm{L}}-\mathrm{L})}}\frac{W_{\nu_{n\mathrm{L}},\mathrm{L}+1/2}(x)}{x}, \tag{11}$$

where $\Gamma(z)$ is the gamma function,

$$L^{2\lambda+1}_{n_r}(x) = \frac{(2\lambda+2)_{n_r}}{n_r!}\sum_{k=0}^{n_r}\frac{(-n_r)_k}{k!(2\lambda+2)_k}x^k \tag{12}$$

is the generalized Laguerre polynomial [26], the argument $x = 2Zr/\nu_{n\mathrm{L}}$ includes the Rydberg electron radial variable $r$, and the effective principal quantum number $\nu_{n\mathrm{L}} \equiv n - \mu_{n\mathrm{L}} = Z/\sqrt{-2E_{n\mathrm{L}}}$, related to the effective orbital $\lambda = \nu_{n\mathrm{L}} - n_r - 1$ and radial $n_r = 0, 1, 2, \ldots$ quantum numbers [11,17], $Z$ is the charge of residual ion ($Z$ = 1 for a neutral atom), and $(a)_k = \Gamma(a+k)/\Gamma(a) = a\cdot(a+1)\cdot\ldots\cdot(a+k-1)$ is the Pochhammer symbol [26]. The integer value $n_r$ determines the power of the Laguerre polynomial (12). Here, $E_{n\mathrm{L}} = -Z^2/\left(2\nu^2_{n\mathrm{L}}\right)$ is the Rydberg-state energy.

The Whittaker function of Equation (11) may be also presented in terms of a hypergeometric polynomial [26,27]

$${}_2\widetilde{F}_0\left(a_1, a_2; -\frac{1}{x}\right) = \sum_{k=0}^{k_{\max}}\frac{(a_1)_k(a_2)_k}{k!}\left(-\frac{1}{x}\right)^k \tag{13}$$

in the form [25–27]:

$$W_{\nu_{n\mathrm{L}},\mathrm{L}+1/2}(x) = \exp\left(-\frac{x}{2}\right)x^{\nu_{n\mathrm{L}}}{}_2\widetilde{F}_0\left(\mathrm{L}+1-\nu_{n\mathrm{L}}, -\nu_{n\mathrm{L}}; -\mathrm{L}; -\frac{1}{x}\right). \tag{14}$$

The symbol tilde determines the polynomial, including a finite number of terms from an infinite number of terms in the hypergeometric series, corresponding to an asymptotic expansion of the Whittaker function in the vicinity of the origin $r$ = 0. The maximal value of the summation index in (13) (the power of the polynomial) should be taken as $k_{\max} = [\nu_{n\mathrm{L}}]$ to eliminate the singularity of the radial wave function (11) [19]. The brackets $[a]$ indicate the integer part of $a$. Thus, the Whittaker function (14) remains finite at $x = 0$, despite the polynomial (13) singularity.

It is worth noting that the number of terms in the sum (12) $n_r$ may differ essentially from that of the sum (13) $k_{\max}$, since the integer part of the effective principal quantum number $[\nu_{n\mathrm{L}}]$ of states with a large orbital momentum L may exceed the radial quantum number $n_r$. This means that the terms with small powers of the radial variable in functions $R^{(\mathrm{FMP})}_{n\mathrm{L}}(r)$ and $R^{(\mathrm{QDM})}_{n\mathrm{L}}(r)$ in (10) and (11) may be different. Meanwhile, the largest powers of the arguments are identical since $\lambda + n_r = \nu_{n\mathrm{L}} - 1$. Thus, the FMP and QDM functions differ from one another at small distances $r$, and they are practically identical at large distances from the atomic core. Therefore, the values of the matrix elements of dipole transitions between states with close energies, determined using FMP and QDM wave functions, practically coincide with each other. The agreement between the

results of the FMP and QGM improves with an increase in the principal $n$ and orbital L quantum numbers.

Using the wave functions (10) and (11), the integration of the radial matrix elements may be performed in the analytical form and presented in terms of combinations of the hypergeometric functions, such as [27]

$$\begin{aligned}\widetilde{\Sigma}_4(a,b,a',b';c;z,z') &= \sum_{k=0}^{k_{\max}}\sum_{k'=0}^{k'_{\max}} \frac{(a)_k(b)_k(a')_{k'}(b')_{k'}}{k!k'!(c)_{k+k'}} z^k z'^{k'} \\ &= \sum_{k'=0}^{k_{\max}} \frac{(a)_k(b)_k}{k!(c)_k} z^k \, {}_2\widetilde{F}_1(a',b';c+k;z'),\end{aligned} \tag{15}$$

where ${}_2\widetilde{F}_1(a',b';c+k;z')$ is the Gauss hypergeometric function [26]. Finally, the analytic equation for the radial matrix element reads

$$\langle n'\mathrm{L}'|r|n\mathrm{L}\rangle = \frac{x^{\nu'+1}(x')^{\nu+1}\Gamma(\nu+\nu'+2)\widetilde{\Sigma}_4(a,b,a',b';c;1/x,1/x')}{4Z\sqrt{\Gamma(\nu+\mathrm{L}+1)\Gamma(\nu-\mathrm{L})\Gamma(\nu'+\mathrm{L}'+1)\Gamma(\nu'-\mathrm{L}')}}, \tag{16}$$

where $x = 2\nu'/(\nu+\nu')$, $x' = 2\nu/(\nu+\nu')$, $a = \mathrm{L}+1-\nu$, $b = -\mathrm{L}-\nu$, $a' = \mathrm{L}'+1-b = -\mathrm{L}-\nu'$, $b' = -\mathrm{L}'-\nu'$, $c = -1-\nu-\nu'$. This equation was first presented in [27] with minor misprints, but when calculating numerical data, the correct Equation (16) was used. A similar equation for the radial matrix elements in terms of the hypergeometric polynomials of two variables may also be derived with the use of the FMP wave functions (see, for example, Section 4.5 of the reference [17]). The difference between the data of the QDM and FMP approaches does not exceed the uncertainties of the 1–3% characteristic of the semiempirical methods based on currently available data for atomic energy levels. The values of the parameters of the functions (10) and (11) are determined from the energy spectra of the $^1S_0$, $^1P_1$, $^1D_2$, and $^1F_3$ series of states of a given atom. For Rydberg states, the effective quantum numbers were calculated using the numerical values of the corresponding quantum defects, as presented in Section 3.

The results of the numerical computations with the use of Equations (15) and (16) for the matrix elements of the μw dipole transitions between Rydberg states with principal quantum numbers in the region from $n$ = 10 to $n$ = 250 are in good agreement with the existing data in the literature, with a fractional departure below 1%. The values of the matrix elements (9) may be conveniently approximated by a quadratic polynomial in the powers of the corresponding principal quantum number as follows:

$$\mathcal{R}(n) = a_0 + a_1 n + a_2 n^2. \tag{17}$$

The coefficients $a_0$, $a_1$, and $a_2$, presented in Tables 6–9, are determined with the use of the standard curve fitting interpolation polynomial procedure for the calculated values of the matrix elements at $n$ = 50, 100, and 150.

A comparison of the numerical values given by approximation (17) with matrix elements calculated in the FMP and QDM approaches confirms its high precision for all considered transitions in atoms; the fractional differences between calculated and approximated values do not exceed 0.1% in the regions of principal quantum numbers from 15 to 500.

**Table 6.** Numerical values (in atomic units) and coefficients of the quadratic polynomial presentation (17) for the matrix elements of electrodipole transitions between the Rydberg states of ***Zn*** atoms. The bra-vector states are the states of higher energy, and the ket-vector states are the lower-energy states. Corresponding transition frequencies are presented in Table 2.

| $n$ | $\langle n^1S_0\|z\|(n-1)^1P_1\rangle$ | $\langle n^1P_1\|z\|n^1S_0\rangle$ | $\langle (n+1)^1P_1\|z\|n^1D_2\rangle$ | $\langle n^1D_2\|z\|(n-2)^1F_3\rangle$ | $\langle (n-1)^1F_3\|z\|n^1D_2\rangle$ |
|---|---|---|---|---|---|
| 20 | 192.207 | 192.940 | 264.753 | 94.0656 | 262.173 |
| 50 | 1484.28 | 1378.05 | 1799.39 | 728.350 | 1742.94 |
| 100 | 6336.07 | 5756.48 | 7391.21 | 3102.77 | 7101.89 |
| 150 | 14,560.5 | 13,138.9 | 16,775.5 | 7123.17 | 16,075.02 |
| 200 | 26,157.7 | 23,525.3 | 29,952.4 | 12,789.5 | 28,662.3 |
| Coefficients of interpolation polynomial (17) | | | | | |
| $a_0$ | 5.19040 | 3.61539 | 0.0868455 | −0.104969 | −1.85717 |
| $a_1$ | −4.14509 | −2.55116 | −1.93900 | −1.89060 | −1.24583 |
| $a_2$ | 0.674539 | 0.600798 | 0.758503 | 0.329194 | 0.722833 |

**Table 7.** Same, as in Table 6, for ***Cd*** atoms. Corresponding transition frequencies are presented in Table 3.

| $n$ | $\langle n^1S_0\|z\|(n-1)^1P_1\rangle$ | $\langle n^1P_1\|z\|n^1S_0\rangle$ | $\langle (n+1)^1P_1\|z\|n^1D_2\rangle$ | $\langle n^1D_2\|z\|n^1P_1\rangle$ | $\langle (n-2)^1F_3\|z\|n^1D_2\rangle$ |
|---|---|---|---|---|---|
| 20 | 180.176 | 160.779 | 233.531 | 100.911 | 236.081 |
| 50 | 1515.662 | 1209.88 | 1703.78 | 704.385 | 1684.28 |
| 100 | 6616.56 | 5150.60 | 7151.06 | 2918.56 | 7013.87 |
| 150 | 15,311.4 | 11,831.0 | 16,344.04 | 6643.98 | 15,988.4 |
| 200 | 27,600.1 | 21,251.2 | 29,282.7 | 11,880.7 | 28,607.9 |
| Coefficients of interpolation polynomial (17) | | | | | |
| $a_0$ | 8.67569 | 8.89962 | 2.19374 | 1.46048 | −0.335623 |
| $a_1$ | −5.79943 | −3.37771 | −3.42512 | −1.05397 | −2.75730 |
| $a_2$ | 0.718783 | 0.547947 | 0.749138 | 0.302249 | 0.728994 |

**Table 8.** Same, as in Table 6, for ***Hg*** atoms. Corresponding transition frequencies are presented in Table 4.

| $n$ | $\langle n^1S_0\|z\|(n-1)^1P_1\rangle$ | $\langle n^1P_1\|z\|n^1S_0\rangle$ | $\langle (n+1)^1P_1\|z\|n^1D_2\rangle$ | $\langle n^1D_2\|z\|n^1P_1\rangle$ | $\langle (n-2)^1F_3\|z\|n^1D_2\rangle$ |
|---|---|---|---|---|---|
| 20 | 162.316 | 137.992 | 218.701 | 64.7528 | 215.642 |
| 50 | 1450.13 | 1158.34 | 1698.30 | 445.609 | 1670.54 |
| 100 | 6464.05 | 5061.94 | 7258.25 | 1859.08 | 7127.96 |
| 150 | 15,061.8 | 11,718.3 | 16,685.6 | 4245.68 | 16,375.9 |
| 200 | 27,243.4 | 21,127.4 | 29,980.3 | 7605.33 | 29,414.4 |
| Coefficients of interpolation polynomial (17) | | | | | |
| $a_0$ | 20.0746 | 7.51134 | 5.75189 | 5.25138 | 3.66453 |
| $a_1$ | −7.23740 | −4.51134 | −4.82297 | −0.924042 | −4.56784 |
| $a_2$ | 0.716772 | 0.550557 | 0.773479 | 0.194624 | 0.758108 |

**Table 9.** Same, as in Table 6, for ***Yb*** atoms. Corresponding transition frequencies are presented in Table 5.

| $n$ | $\langle n^1S_0\|z\|(n-1)^1P_1\rangle$ | $\langle n^1P_1\|z\|n^1S_0\rangle$ | $\langle n^1D_2\|z\|(n+1)^1P_1\rangle$ | $\langle n^1D_2\|z\|(n-2)^1F_3\rangle$ | $\langle (n-1)^1F_3\|z\|n^1D_2\rangle$ |
|---|---|---|---|---|---|
| 20 | 101.472 | 201.632 | 216.582 | 136.886 | 193.186 |
| 50 | 943.043 | 1642.07 | 1610.04 | 1091.50 | 1398.82 |
| 100 | 4213.32 | 7143.57 | 6801.84 | 4721.86 | 5841.46 |
| 150 | 9818.61 | 16,519.6 | 15,580.7 | 10,901.4 | 13,324.6 |
| 200 | 17,758.9 | 29,770.0 | 27,946.6 | 19,630.0 | 23,848.1 |
| Coefficients of interpolation polynomial (17) | | | | | |
| $a_0$ | 7.79825 | 15.0819 | 5.30766 | 10.2918 | −3.32539 |
| $a_1$ | −4.64536 | −6.20523 | −3.77607 | −3.86720 | −2.36219 |
| $a_2$ | 0.467005 | 0.774901 | 0.717413 | 0.509829 | 0.608100 |

## 5. Discussions

The interest in the highly excited states of the alkaline–earth–metal-like neutral Yb atom appeared in the 1980s, both in experimental and theoretical research [28–30]. In the 1990s, this interest reappeared and continued until the present day [22,31,32]. The interest in Rydberg-state Yb and alkaline–earth–metal-like atoms of group IIb elements is related, first of all, with the long-range interaction inducing practically important effects of Rydberg blockade [12] and electromagnetically induced transparency [33–35] of atomic gases, usually demonstrating strong opacity with respect to resonant light waves.

Due to the rather small amount of literature on the Rydberg-state energy levels of group IIb atoms, we had to use the databases of [13,14] for deriving quantum defects, presented in Table 1, for a series of singlet states with angular momenta L $\leq$ 3. Thus, the data on transition frequencies between the closest $^1S_0$, $^1P_1$, $^1D_2$, and $^1F_3$ states were extended to Rydberg states with practically arbitrarily large principal quantum numbers $n$. The data in Tables 2–5 and Equation (8) provide useful tools for determining the numerical values of the Rydberg–Rydberg dipole transition frequencies, which are absent in the current literature to date.

The high sensitivity of Rydberg states to static fields may influence the frequencies of the μw transitions calculated in Section 3 of this paper. Therefore, in measuring these frequencies, one should carefully reduce all residual, accidental, and stray fields of the laboratory apparatus, which could distort the measurement data. However, it is useful to bear in mind that the Stark shifts induced by intense high-frequency laser fields are nearly equal for all Rydberg states, conserving the immunity of the calculated transition frequencies in Section 2 to the field of the coupling waves.

Meanwhile, the intense coupling waves also influence the ground $n_0{}^1S_0$ and resonance $n_0{}^1P_1$ states, leading to the Stark shift of the absorbed probe radiation, thereby inducing the additional shifts of absorption and transparency for the probe wave. This effect should be taken into account together with the actions of environmental laboratory fields.

It is also worth noting that the data in Tables 1–9 may be useful for determining the most suitable atom and frequency of transition between its Rydberg states for evaluating the transition–amplitude-dependent efficiency in measuring the characteristics of the corresponding μw radiation. In this regard, the most important quantity that determines the transition amplitude is the coefficient $a_2$ of the quadratic polynomial (17). In particular, the maximal values of the transition amplitudes in the Zn, Cd, and Hg atoms correspond to $(n+1)^1P_1 \rightarrow n^1D_2$ transitions. In Yb atoms, the maximal amplitudes correspond to the transitions $n^1P_1 \rightarrow n^1S_0$.

## 6. Conclusions

The main results of this paper are the numerical data for the basic characteristics of group IIb (Zn, Cd, Hg) and Yb atoms dipole radiation transitions from Rydberg state $n^1L_L$ to the close energy states of opposite parity $n'^1L'_{L'}$ (where $L' = L \pm 1$, $|n' - n| \leq 2$). The corresponding frequencies were determined for microwaves (μw), which are sometimes also called radio frequency (RF) or millimeter waves in the literature [23,24]. The most reliable data in the literature on energy levels were used to determine the quantum defects of $n^1S_0$, $n^1P_1$, $n^1D_2$, and $n^1F_3$ series of states (see Table 1) used for calculating the frequencies of transitions between highly excited Rydberg states. Equation (8) for the Rydberg–Rydberg transition frequencies as functions of the principal quantum number $n$ was derived using the curve fitting interpolation polynomial approach with the coefficients shown in Tables 2–5. This equation allows simple evaluations of frequencies for relevant electric dipole transitions between Rydberg states with close principal quantum numbers in the alkaline–earth–metal-like atoms.

The matrix elements of transitions $\mathcal{R} = \langle n'|z|n\rangle$ were calculated using the semi-empirical methods of Fues' model potential (FMP) and the quantum defect method (QDM). The calculated numerical data demonstrated significant equivalence between the two methods; the fractional departure between the corresponding matrix elements did not exceed 0.1% in the region of the quantum number values $n > 15$. Therefore, only the results of the calculations in the QDM are presented in Tables 6–9. The data for the matrix elements correspond to the transitions for which the data on frequencies may be found in Tables 2–5. The curve fitting interpolation procedure, based on the numerical data for $\mathcal{R}(n)$ at $n$ = 50, 100, and 150, was used for deriving the polynomials of the asymptotic presentation (17). The coefficients of the polynomials are listed for each transition in Tables 6–9, thereby providing interpolated numerical values of matrix elements with a fractional departure from computed in the QDM approach data below 0.1% in the region of the principal quantum numbers $n$ between 15 and 500.

In summary, the calculated results of this study provide new information on the frequencies and matrix elements of transitions between the highly excited Rydberg states of alkaline–earth–metal-like atoms, which so far are presented in the literature only for particular states of alkali and alkaline–earth–metal atoms [10,11]. The calculated numerical data may provide important information for planning further research on the use of Rydberg atoms for the development of new methods of μw radiation metrology and for constructing Rydberg-atom-based radio frequency systems for digital communications [36,37].

In addition to the effects on Rydberg singlet states of group IIb atoms and Yb, discussed in this paper, and those of group IIa, presented in [11], similar effects on triplet states may attract interest [38] and should be considered in future research.

**Author Contributions:** Conceptualization, V.D.O. and V.G.P.; methodology, V.D.O. and V.G.P.; software, V.D.O. and I.L.G.; validation V.D.O., A.A.K. and I.L.G.; formal analysis, V.D.O. and V.G.P.; investigation, V.D.O. and V.G.P.; resources, V.G.P.; data curation, V.D.O., A.A.K. and I.L.G.; writing—original draft preparation, V.D.O.; writing—review and editing, V.D.O., A.A.K. and I.L.G.; visualization, I.L.G.; supervision, V.G.P.; project administration, V.G.P.; funding acquisition, V.D.O. and V.G.P. All authors have read and agreed to the published version of the manuscript.

**Funding:** The Ministry of Science and Higher Education of the Russian Federation (Project FZGU-2023-0007).

**Institutional Review Board Statement:** Not applicable.

**Informed Consent Statement:** Not applicable.

**Data Availability Statement:** Not applicable.

**Acknowledgments:** This study was supported in part by the Ministry of Science and Higher Education of the Russian Federation within the framework of the State Assignment (Project FZGU-2023-0007).

**Conflicts of Interest:** The authors declare no conflict of interest.

## References


1. Ludlow, A.D.; Boyd, M.M.; Ye, J.; Peik, E.; Schmidt, P.O. Optical atomic clocks. *Rev. Mod. Phys.* **2015**, *87*, 637. [CrossRef]
2. Ushijima, I.; Takamoto, M.; Katori, H. Operational Magic Intensity for Sr Optical Lattice Clocks. *Phys. Rev. Lett.* **2018**, *121*, 263202. [CrossRef]
3. Takeuchi, R.; Chiba, H.; Okaba, S.; Takamoto, M.; Tsuji, S.; Katori, H. Continuous outcoupling of ultracold strontium atoms combining three different traps. *Appl. Phys. Express* **2023**, *16*, 042003. [CrossRef]
4. Mohapatra, A.K.; Jackson, T.R.; Adams, C.S. Coherent optical detection of highly excited Rydberg states using electromagnetically induced transparency. *Phys. Rev. Lett.* **2007**, *98*, 113003. [CrossRef]
5. Sedlacek, J.A.; Schwettmann, A.; Kubler, H.; Low, R.; Pfau, T.; Shaffe, J.P. Microwave electrometry with Rydberg atoms in a vapour cell using bright atomic resonances. *Nat. Phys.* **2012**, *8*, 819–824. [CrossRef]
6. Holloway, C.L.; Gordon, J.A.; Jefferts, S.; Schwarzkopf, A.; Anderson, D.A.; Miller, S.A.; Thaicharoen, N.; Raithel, G. Broadband Rydberg Atom-Based Electric-Field Probe for SI-Traceable, Self-Calibrated Measurements. *IEEE Trans. Antennas Propag.* **2014**, *62*, 6169–6182. [CrossRef]
7. Holloway, C.L.; Simons, M.T.; Gordon, J.A.; Wilson, P.F.; Cooke, C.M.; Anderson, D.A.; Raithel, G. Atom-Based RF Electric Field Metrology: From Self-Calibrated Measurements to Subwavelength and Near-Field Imaging. *IEEE Trans. Electromagn. Compat.* **2017**, *59*, 717–728. [CrossRef]
8. Kumar, S.; Fan, H.; Kubler, H.; Sheng, J.; Shaffer, J.P. Atom-based sensing of weak radio frequency electric fields using homodyne readout. *Sci. Rep.* **2017**, *7*, 42981. [CrossRef]
9. Simons, M.T.; Gordon, J.A.; Holloway, C.L. Fiber-coupled vapor cell for a portable Rydberg atom-based radio frequency electric field sensor. *Appl. Opt.* **2018**, *57*, 6456–6460. [CrossRef]
10. Ovsiannikov, V.D.; Palchikov, V.G.; Glukhov, I.L. Microwave field metrology based on Rydberg states of alkali-metal atoms. *Photonics* **2022**, *9*, 635. [CrossRef]
11. Glukhov, I.L.; Kamenski, A.A.; Ovsiannikov, V.D.; Palchikov, V.G. Precision spectroscopy of alkaline-earth atom Rydberg states for determining characteristics of microwave radiation. *ZHETP* **2023**, *164*, 193–203.
12. Dunning, F.B.; Killian, T.C.; Yoshida, S.; Burgdorfer, J. Recent advances in Rydberg physics using alkaline-earth atoms. *J. Phys. B At. Mol. Opt. Phys.* **2016**, *49*, 112003. [CrossRef]
13. Kramida, A.; Ralchenko, Y.; Reader, J.; NIST ASD Team. *NIST Atomic Spectra Database (Version 5.9)*; National Institute of Standards and Technology: Gaithersburg, MD, USA, 2021. [CrossRef]
14. Kazakov, V.V.; Kazakov, V.G.; Kovalev, V.S.; Meshkov, O.I.; Yatsenko, A.S. Electronic structure of atoms: Atomic spectroscopy information system. *Phys. Scr.* **2017**, *92*, 10. Available online: http://grotrian.nsu.ru (accessed on 25 August 2023). [CrossRef]
15. Autler, S.H.; Townes, C.H. Stark effect in rapidly varying fields. *Phys. Rev.* **1955**, *100*, 703–722. [CrossRef]
16. Landau, L.D.; Lifshitz, E.M. *Quantum Mechanics: Nonrelativistic Theory*, 3rd ed.; *§ 39*; Butterworth-Heinemann: Oxford, UK, 1981; ISBN 978-0750635394. Available online: https://www.amazon.com/Quantum-Mechanics-Non-Relativistic-Theory-3/dp/0750635398 (accessed on 25 August 2023).
17. Manakov, N.L.; Ovsiannikov, V.D.; Rapoport, L.P. Atoms in a laser field. *Phys. Rep.* **1986**, *141*, 319–433. [CrossRef]
18. Stelmashenko, E.F.; Klezovich, O.A.; Baryshev, V.N.; Tishchenko, V.A.; Blinov, I.Y.; Palchikov, V.G.; Ovsiannikov, V.D. Measuring the electric field strength of microwave radiation at the frequency of the radiation transition between Rydberg states of atoms $^{85}$Rb. *Opt. Spectrosc.* **2020**, *128*, 1067–1073. [CrossRef]
19. Sobelman, I.I. *An Introduction to the Theory of Atomic Spectra*, 1st ed.; Pergamon Press: London, UK, 1972; ISBN 9781483159720. Available online: https://www.elsevier.com/books/introduction-to-the-theory-of-atomic-spectra/sobelman/978-0-08-016166-2 (accessed on 25 August 2023).
20. Robicheaux, F. Calculations of long range interactions for $^{87}$Sr Rydberg states. *J. Phys. B* **2019**, *52*, 244001. [CrossRef]
21. Martin, W.C. Series formulas for the spectrum of atomic sodium. *J. Opt. Soc. Am.* **1980**, *70*, 784–788. [CrossRef]
22. Lehec, H.; Zuliani, A.; Maineult, W.; Luc-Koenig, E.; Pillet, P.; Cheinet, P.; Niyaz, F.; Gallagher, T.F. Laser and microwave spectroscopy of even-parity Rydberg states of neutral ytterbium and multichannel-quantum-defect-theory analysis. *Phys. Rev. A* **2018**, *98*, 062506. [CrossRef]
23. Kutsenko, A.S.; Dyubko, S.F.; Pogrebnyak, N.L. Millimeter-wave spectroscopy of Zn I in triplet F Rydberg states. *Spectrochim. Acta Part B* **2019**, *160*, 105674. [CrossRef]
24. Dyubko, S.F.; Pogrebnyak, M.L.; Kutsenko, A.S. Millimeter-wave spectroscopy of neutral mercury in Rydberg F states. *Spectrosc. Lett.* **2021**, *54*, 375–380. [CrossRef]
25. Varshalovich, D.A.; Moskalev, A.N.; Khersonskii, V.K. *Quantum Theory of Angular Momentum*; Ebook for Individuals; World Scientific: Singapore, 1988; ISBN 978-981-4578-28-8. Available online: https://www.worldscientific.com/worldscibooks/10.1142/0270#t=aboutBook (accessed on 25 August 2023).
26. Bateman, H.; Erdelyi, A. *Higher Transcendental Functions*; Volumes I, II, McGraw-Hill Book Company: New York, NY, USA, 1953; Available online: https://authors.library.caltech.edu/43491/ (accessed on 25 August 2023).
27. Glukhov, I.L.; Kamenski, A.A.; Ovsiannikov, V.D. The use of photoionization cross section for evaluating contribution of continuum to the blackbody radiation induced shift and broadening of Rydberg-state energy levels of group IIb ions. *J. Quant. Spectrosc. Rad. Trans.* **2022**, *280*, 108068. [CrossRef]

28. Camus, P.; Débarre, A.; Morillon, C. Highly excited levels of neutral ytterbium I. Two-photon and two-step spectroscopy of even spectra. *J. Phys. B* **1980**, *13*, 1073.
29. Aymar, M.; Débarre, A.; Robaux, O. Highly excited levels of neutral ytterbium II. Multichannel quantum defect of odd- and even-parity spectra. *J. Phys. B* **1980**, *13*, 1089.
30. Aymar, M.; Champeau, R.J.; Delsart, C.; Robaux, O. Three-step laser spectroscopy and multichannel quantum defect analysis of odd-parity Rydberg states of neutral ytterbium. *J. Phys. B* **1984**, *17*, 3645.
31. Bowers, C.J.; Budker, D.; Commins, E.D.; DeMille, D.; Freedman, S.J.; Nguyen, A.-T.; Shang, S.-Q.; Zolotorev, M. Experimental investigation of excited-state lifetimes in atomic ytterbium. *Phys. Rev. A* **1996**, *53*, 3103.
32. Ali, R.; Yaseen, M.; Nadeem, A.; Bhatti, S.A.; Baig, M.A. Two-colour three-photon excitation of the 6s*n*f $^{1,3}F_3$ and 6s*n*p $^1P_1$, $^3P_{1,2}$ Rydberg levels of Yb I. *J. Phys. B* **1999**, *32*, 953.
33. Boiler, K.-J.; Imamoglu, A.; Harris, S.E. Observation of Electromagnetically Induced Transparency. *Phys. Rev. Lett.* **1991**, *66*, 2593.
34. Novikova, I.; Walsworth, R.L.; Xiao, Y. Electromagnetically induced transparency-based slow and stored light in warm atoms. *Laser Photonics Rev.* **2012**, *6*, 333. [CrossRef]
35. Guo, Y.-W.; Xu, S.-L.; He, J.-R.; Deng, P.; Belic, M.R.; Zhao, Y. Transient optical response of cold Rydberg atoms with electromagnetically induced transparency. *Phys. Rev. A* **2018**, *101*, 023806.
36. Song, Z.; Liu, H.; Liu, X.; Zhang, W.; Zou, H.; Zhang, J.; Qu, J. Rydberg-atom-based digital communication using a continuously tunable radio-frequency carrier. *Opt. Express* **2019**, *27*, 8848–8857. [CrossRef] [PubMed]
37. Song, Z.; Feng, Z.; Liu, X.; Li, D.; Zhang, H.; Liu, J.; Zhang, L. Quantum-based determination of antenna finite range gain by using Rydberg atoms. *IEEE Antennas Wirel. Propag. Lett.* **2017**, *16*, 1589–1592. [CrossRef]
38. Zhou, Y.-L.; Yan, D.; Li, W. Rydberg electromagnetically induced transparency and absorption of strontium triplet states in a weak microwave field. *Phys. Rev. A* **2022**, *105*, 053714. [CrossRef]